ACS APPLIED MATERIALS & INTERFACES

www.acsami.org

Research Article

Airflow Enhanced Solar Evaporation Based on Janus Graphene Membranes with Stable Interfacial Floatability

Dong-Dong Han, Zhao-Di Chen, Ji-Chao Li, Jiang-Wei Mao, Zhi-Zhen Jiao, Wei Wang, Wei Zhang, Yong-Lai Zhang,* and Hong-Bo Sun

Cite This: ACS Appl. Mater. Interfaces 2020, 12, 25435−25443

Read Online

ACCESS | Metrics & More | Article Recommendations | Supporting Information

ABSTRACT: Solar interfacial evaporation has been recognized as a versatile energy conversion protocol for cutting-edge applications such as water treatment and power generation (e.g., hydro voltaic effect). Recently, to enhance water evaporation rates, water temperature and evaporation area have been considered as essential ingredients, and thus photothermal materials and three-dimensional hierarchical structures have been developed to promote light-to-heat conversion efficiency and enhance interfacial evaporation. However, less attention has been paid to the airflow effect, because the interfacial floatability of photothermal membranes should be considered under air blast. Here, inspired from the stable interfacial floatability of lotus leaves, we report the airflow enhanced solar interfacial evaporation approach using a graphene-based Janus membrane. Laser-induced graphene (LIG) film was treated unilaterally by O_2 plasma, forming a LIG/oxidized LIG (LIG-O) Janus membrane with distinct wettability on two sides. Higher water evaporation rate of 1.512 kg m^{-2} h^{-1} is achieved. The high solar interfacial evaporation performance can be attributed to the two advantages: (i) the combination of microscale capillary water transporting and nanoscale light trapping; (ii) hydrophobic/hydrophilic Janus membrane for stable interfacial floatability under airflow. Our approach is feasible for developing high-performance solar interfacial evaporation devices for practical clean energy utilization.

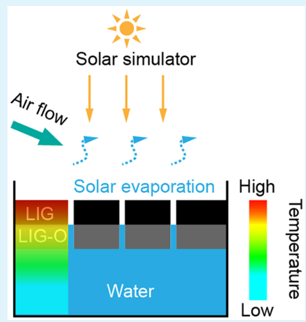

KEYWORDS: *solar evaporation, air flowing enhancement, Janus membrane, interfacial floatability, laser-induced graphene*

1. INTRODUCTION

As a versatile energy conversion protocol, solar interfacial evaporation has attracted significant interest in water treatment and power generation (e.g., hydro voltaic effect).[1−5] In a typical solar interfacial evaporation process, an absorber converts solar radiation energy into heat effectively.[6−8] Meanwhile, certain heat locations can vaporize water and allow the as-generated vapor to escape.[9,10] Initially, various photothermal materials with high light-to-heat conversion efficiencies have been developed for solar interfacial evaporation, for instance plasmonic metal nanoparticles, semiconducting materials, and carbon materials.[11−16] Subsequently, to further promote the evaporation efficiency, three-dimensional (3D) photothermal structures, such as rose-, cone-, and cylindrical cup-shaped structures, have been fabricated, demonstrating enhanced water evaporation rates because of greater internal light reflection and improved transpiration pathways.[17−21] In most implementations, the photothermal material is arranged to cover the entire surface of the water vessel. For a lab-scale study, it seems that it is unnecessary to control the wettability of the photothermal materials since it cannot move laterally. Recently, to advance salt resistance for desalination, multilayered hydrophobic/hydrophilic structures have been fabricated by coating,[22,23] filtration,[24−26] electric spinning,[27,28] and freeze-drying technology.[29−31] For example, Darling et al. have reported highly-efficiency solar steam generation based on novel Janus membranes or powerful photothermal materials.[32−34] Zhang et al. have creatively demonstrated a double-layer flamed corn straw in a significantly low cost for a solar-driven interfacial evaporator.[35] Nowadays, to develop solar absorbers with higher evaporation rate and salt resistant, efforts have been devoted to prepare highly efficient photothermal materials that feature low cost, broadband absorption, robustness, and superwettability.

Graphene is a versatile material that offers high photothermal conversion efficiency, tunable wettability, mechanical strength, and ease of functionalization.[36−40] Recently, significant efforts have been devoted to graphene-based solar interfacial evaporation absorbers.[41−45] For example, to efficiently heat up a graphene absorber, Qu et al. successfully developed graphene absorbers by combining the photo/electro-to-heat effect of graphene for highly efficient solar interfacial evaporation.[46] Subsequently, to facilitate water transportation to heat locations, vertically aligned graphene sheet membranes have been fabricated via freeze-drying/

Received: March 23, 2020
Accepted: May 13, 2020
Published: May 13, 2020

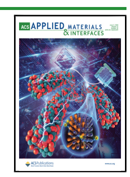

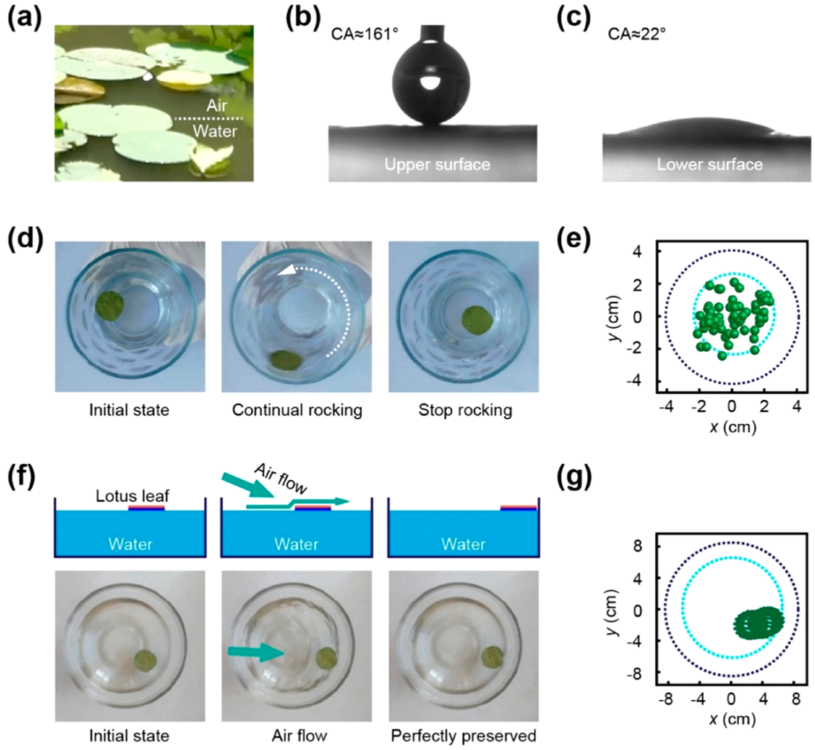

Figure 1. Janus wettability and antirotating and windproof abilities of floating lotus leaves. (a) Optical image of floating lotus leaves. Water contact angle (CA) images of (b) upper and (c) lower surfaces. (d) Antirotating ability. A floating lotus leaf remains as its initial state after the rocking of the water surface. (e) The corresponding trajectory of the lotus leaf centers (the green point) during the antirotating test. (f) Schematics of the windproof ability. (g) The corresponding trajectory of the lotus leaf peripheries (the green circle) during the windproof test. In panels e and g, the blue circle is the edge of water and the purple circle is the edge of the container.

thermal annealing or the injection control technique.[47,48] More importantly, to further enhance the optical absorption of absorbers and expose large areas for vapor dissipation, Zhu et al. successfully achieved 3D graphene oxide (GO) based artificial cone absorbers that can receive wide-ranged incident light.[49−51] Hu et al. creatively reported jellyfish-like GO pillar evaporators via a vertical 3D printing technique.[52,53] In fact, the rate of solar interfacial evaporation depends significantly on water temperature, water evaporation area, and air flow rate.[9,54−57] Currently, the aforementioned excellent works focused on solar interfacial evaporation enhancement by increasing water temperature and evaporation area. However, the influence of air flow rate has been rarely considered in solar interfacial evaporation enhancement. This negligence may be attributed to the interfacial floatability problem of absorber membranes under air blast. From the practical point of view, stable floatability is quite important because there are always big waves and winds in the sea. Especially, for large-area seawater evaporation, a large number of photothermal films would be employed, and the situation would become more obvious.

In this study, inspired by the lotus leaves that possess a superhydrophobic/superhydrophilic integrated Janus wettability, we designed and fabricated a Janus graphene membrane with stable interfacial floatability for solar interfacial evaporation enhancement. The Janus graphene membrane is prepared by laser-induced graphene (LIG) and unilateral O_2 plasma treatment. Taking advantage of the hydrophobic/hydrophilic characteristics and unique materials properties, the LIG and oxidized LIG (LIG-O) Janus membranes enable solar interfacial evaporation by the combining microscale capillary water transporting and nanoscale light trapping. Besides, owing to the improved interfacial floatability, the Janus LIG/LIG-O membranes exhibited antirotating and windproof abilities. Subsequently, the Janus LIG/LIG-O membranes demonstrated remarkably enhanced solar interfacial evaporation performance under airflow condition. Actually, our approach provides the opportunity for developing solar interfacial evaporation devices through new design principles. For instance, a swarm of floating water evaporation devices, just like the lotus leaves, can be fabricated for practical use on the sea. Moreover, in addition to the stable floatability, the distinct wettability on the two sides of the film is also beneficial for other important issues, for instance, the salt resistance during the desalination process. This study provides a state-of-the-art strategy to construct cost-effective, mass-producible, and highly efficient solar interfacial evaporation system toward clean energy utilization.

2. EXPERIMENTAL SECTION

2.1. Preparation of LIG Membrane and LIG/LIG-O Membrane. Laser (P = 1.35 W, DAJA Corporation) scribing on Kapton PI (thickness: 25 μm) was performed prepare LIG. The thickness of LIG membrane is ∼50 μm. After the laser scribing process, Janus graphene membranes (LIG/LIG-O) were prepared by unilateral O_2 plasma treatment of LIG papers for 2 min.

2.2. Solar Evaporation Tests. Solar interfacial evaporation was measured under 1 kW m^{-2}. The LIG and LIG/LIG-O membranes were cut into 1 cm × 1 cm for the solar evaporation test. An electronic balance (LICHEN FA2204) was used to monitor the mass change. An infrared thermometer (FLUKE VT04) was used to measure surface temperatures. The solar thermal conversion efficiency (η) is calculated according to the following equation: $\eta = mh_{LV}/q_i$, where m

https://dx.doi.org/10.1021/acsami.0c05401
ACS Appl. Mater. Interfaces 2020, 12, 25435−25443

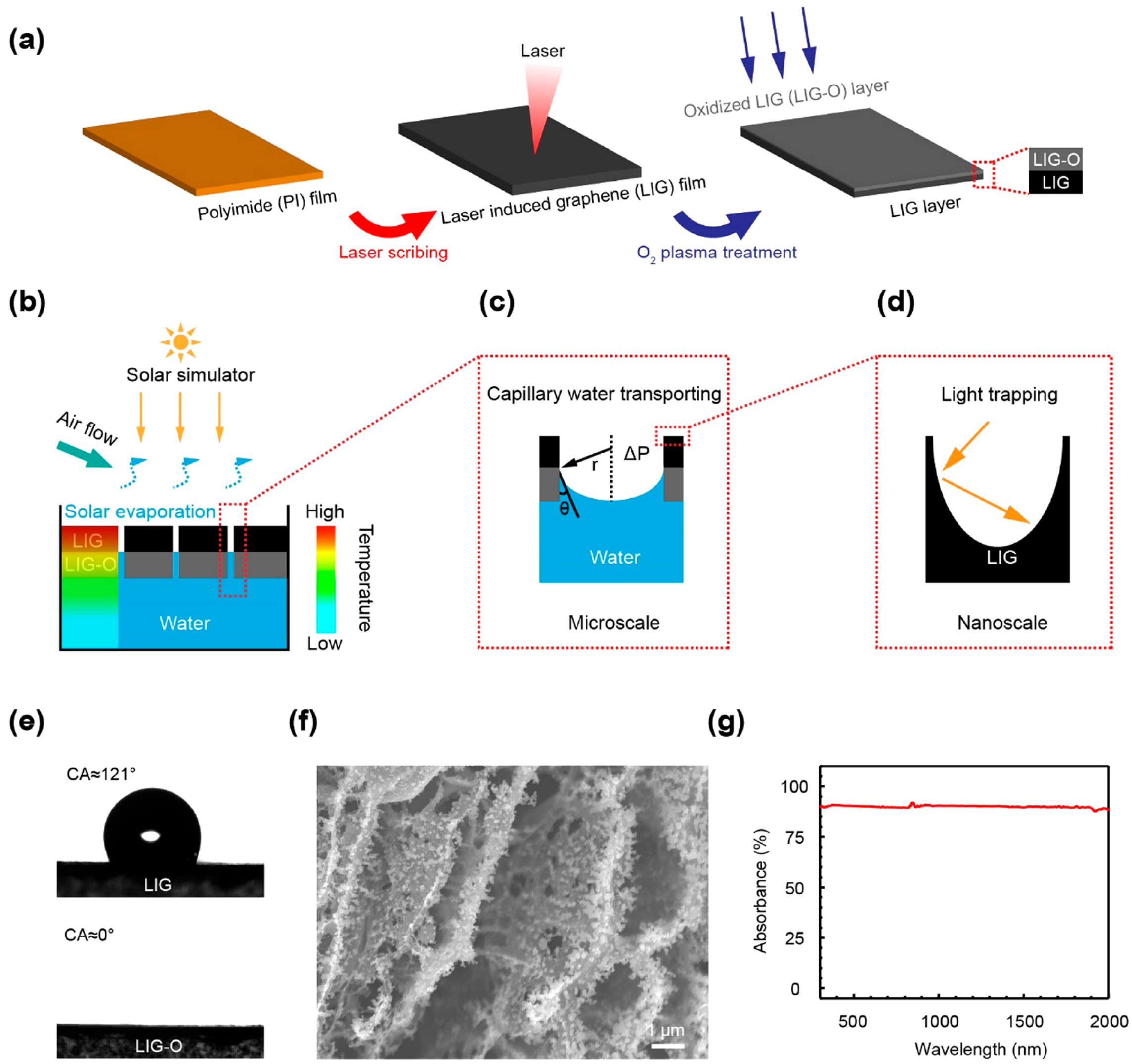

Figure 2. Manufacturing and processing of Janus wettability of LIG/LIG-O membranes for solar interfacial evaporation. Schematics of (a) Janus graphene membrane process and (b) the designed solar interfacial evaporation enhancement system by air flow. (c) Microscale schematic of the capillary water transporting due to the hydrophobic/hydrophilic bilayer structure. (d) Nanoscale light trapping for the top LIG solar absorber. (e) Water-droplet CA images of LIG and LIG-O. (f) Scanning electron microscopy (SEM) image of LIG. (g) Absorption spectrum of LIG.

is the evaporation rate, h_{LV} is the total enthalpy of sensible heat and phase change, and q_i is the solar illumination energy.[2,58,59]

2.3. Characterization. The water-droplet CA were measured by using a contact angle system (SDC-350, SIN DIN Corporation, China). SEM images were obtained using JEOL JSM7500. Raman spectroscopy was obtained using LabRAM HR Evolution. XPS was collected by ESCALAB250 spectrometer. The absorption spectrum of the LIG membrane was obtained using a spectrophotometer (Shimadzu UV-3600).

3. RESULTS AND DISCUSSION

3.1. Stable Interfacial Floatability of Lotus Leaves. Floating on the air−water interface, lotus leaves exhibit evolved special Janus hydrophobic/hydrophilic wettability, which prevents wetting and submersion (Figure 1a−c). To investigate this phenomenon, we measured the water-droplet contact angles (CAs) of the upper and lower surfaces (Figure 1b,c). The upper surface has a large water-droplet CA (∼161°) and the lower surface has a small water-droplet CA (∼22°), demonstrating the Janus wettability. Owing to the hydrophobic air-retaining and hydrophilic water-attaching properties, lotus leaves exhibit antirotating and windproof abilities (Figure 1d−g).[60] As shown in Figure 1d, a floating lotus leaf remained in its initial state after the water surface rocked. The corresponding trajectory of the lotus leaf centers (the green point) during the windproof test is shown in the Figure 1e, and the estimated rotational speed is 1.7 ± 0.2 r/s. The blue circle is the edge of water, and the purple circle is the edge of the container. The rocking lotus leaf can attach on the water surface when the water surface is almost parallel to the wall of the container. In addition, the Janus sheet not only exhibits antirotating ability, but also windproof ability. As illustrated in Figure 1f, air flows over the upper surface. Consequently, the floating lotus leaf can be preserved after air blowing. Figure 1g depicts the corresponding trajectory of the lotus leaf peripheries (the green circle) during the windproof test, of which the average velocity of the lotus leaf is 6.2 ± 0.3 cm/s. In particular, the green circle overlaps the blue circle, which indicates the excellent windproof ability.

3.2. Preparation of Janus Wettability of LIG/LIG-O Membranes. Inspired by the lotus Janus wettability integrated system, Janus graphene membranes were designed and fabricated based on a hydrophobic LIG by combining both

https://dx.doi.org/10.1021/acsami.0c05401
ACS Appl. Mater. Interfaces 2020, 12, 25435−25443

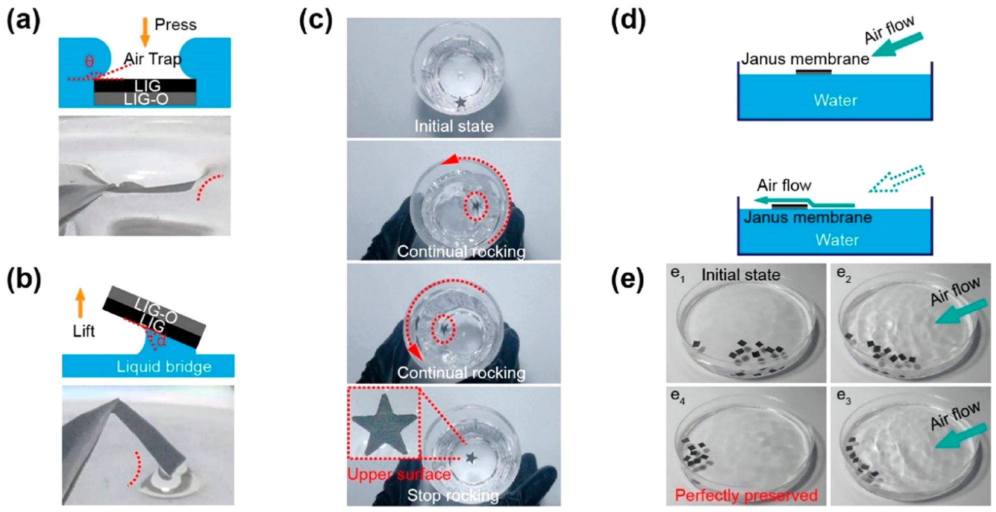

Figure 3. Antirotating and windproof abilities of the Janus LIG/LIG-O membrane. (a and b) Schematic illustration and contact interface between a LIG/LIG-O membrane and water. (c) The Janus LIG/LIG-O membrane remains as its initial state and does not flip over after the rocking of the water surface. (d) Schematics of the windproof ability. (e) The LIG/LIG-O membranes were preserved after wind blowing owing to the Janus wettability of the LIG/LIG-O membrane.

laser scribing technology and unilateral O_2 plasma treatment (Figure 2a). First, commercial polyimide (PI) films were employed as the initial material and laser treatment (P = 1.35 W) was performed prepare structured and porous LIG in an ambient atmosphere. After the laser scribing process, the yellow PI became black LIG (Figure S1) and the black LIG indicated strong light absorption capabilities. The conversion efficiency of laser-induced graphene is ~6.9%. Utilizing the programmable direct laser writing technology, a complex patterned LIG can be easily laser-scribed, e.g., the school badge of Jilin University. To investigate the quality of LIG, Raman spectroscopy was performed. Three prominent peaks were observed including D peak (~1348 cm^{-1}), G peak (~1583 cm^{-1}), and 2D peak (~2703 cm^{-1}; Figure S2). The 2D/G intensity ratio was ~0.76, which indicates the formation of few-layered graphene.[61] Recently, Gong et al. have comprehensively summarized the preparation of graphene from polymer (as carbon source) on Cu or Ni substrate under H_2/Ar flow via chemical vapor deposition method.[63] In our work, LIG is prepared by irradiation of laser on PI film under ambient conditions, PI owns the repeat aromatic and imide repeat units, which plays an important role in the fabrication of LIG. The mechanism of fabrication LIG is because the aromatic compounds rearrange to form graphitic structures after laser treatment.[61] The fabrication of the hydrophilic layer was aided by O_2 plasma treatment. After the O_2 plasma treatment, oxygen containing groups (OCGs) appeared on the LIG nanosheets, resulting in high surface energy. Subsequently, Janus LIG/LIG-O membranes were achieved by unilateral O_2 plasma treatment of LIG membranes. Accordingly, the desired shapes could be laser-cut for solar interfacial evaporation. It is noteworthy that the entire fabrication process of the Janus membrane does not require additional chemical treatments, rendering it a safe and promising device for water purification.

To further evaluate changes in the functional groups of LIG and LIG-O, X-ray photoelectron spectroscopy (XPS) was performed (Figures S3 and S4). During laser scribing, the high temperature could easily break the C−O, C−N, and C═O bonds, and the content of nitrogen is nearly less than 1%.[43,61] After the O_2 plasma treatment of LIG papers, the LIG-O exhibited a higher oxygen content (~19.5%), whereas the LIG a lower oxygen content (~9.56%). In addition, The C 1s XPS spectra of our LIG and LIG-O samples were deconvoluted into three peaks centered at 284.7 (C−C), 286.2 (C−O), and 288.9 eV (C═O; Figure S5).[64] LIG-O exhibited more C−O (~34.4%) and C═O (~11.4%) bonds compared with the LIG (C−O, ~21.2%; C═O, ~4.1%). Consequently, owing to the more oxygen containing groups, the LIG-O became more hydrophilic. It is known that graphene owns high thermal conductivity (~5000 W m^{-1} K^{-1}),[65,66] whereas existing of OCGs on graphene nanosheets would cause a much lower thermal conductivity (~0.2 W m^{-1} K^{-1}), which is beneficial for suppressing the thermal loss down bulk water.[50,67]

The Janus LIG/LIG-O membrane can improve the interfacial floatability. As shown in Figure 2b, the Janus graphene membrane possesses antirotating and windproof abilities and can enhance solar interfacial evaporation by air flow. First, owing to hydrophilicity, bulk water can be supplied through micro channels to the interface between the LIG and LIG-O by capillary force (Figure 2c).[48,68,69] Consequently, the hydrophilic solar interfacial evaporation membrane would transport more water. Therefore, the hydrophobic LIG layer with porous structures contributes significantly to vapor escape and light absorption. In fact, nanoscale structures can trap light, which is significant for light absorption enhancement (Figure 2d).[70,71] In addition, graphene might convert sunlight into heat by electron−hole generation/relaxation or thermal vibration of molecules.[5,9,72,73] To further confirm the wettability difference, we tested the static CAs of the LIG and LIG-O surfaces (Figure 2e). The LIG surface indicated hydrophobicity (static CA ≈ 121°), which was attributed to the low surface energy of the carbon materials (Figures S3−S5) and the microstructures (Figure 2f). Meanwhile, owing to numerous OCGs on the LIG, LIG-O exhibited super-hydrophobicity (static CA ≈ 0°). The morphology of LIG surfaces is rough at the nanoscale and reveals porous structures due to the rapid liberation of gaseous products (Figure 2f). It is noteworthy that the microstructure of photothermal materials indeed influence the performance of solar vapor generation.[62] The morphology and microstructure of LIG can be controlled

https://dx.doi.org/10.1021/acsami.0c05401
ACS Appl. Mater. Interfaces 2020, 12, 25435−25443

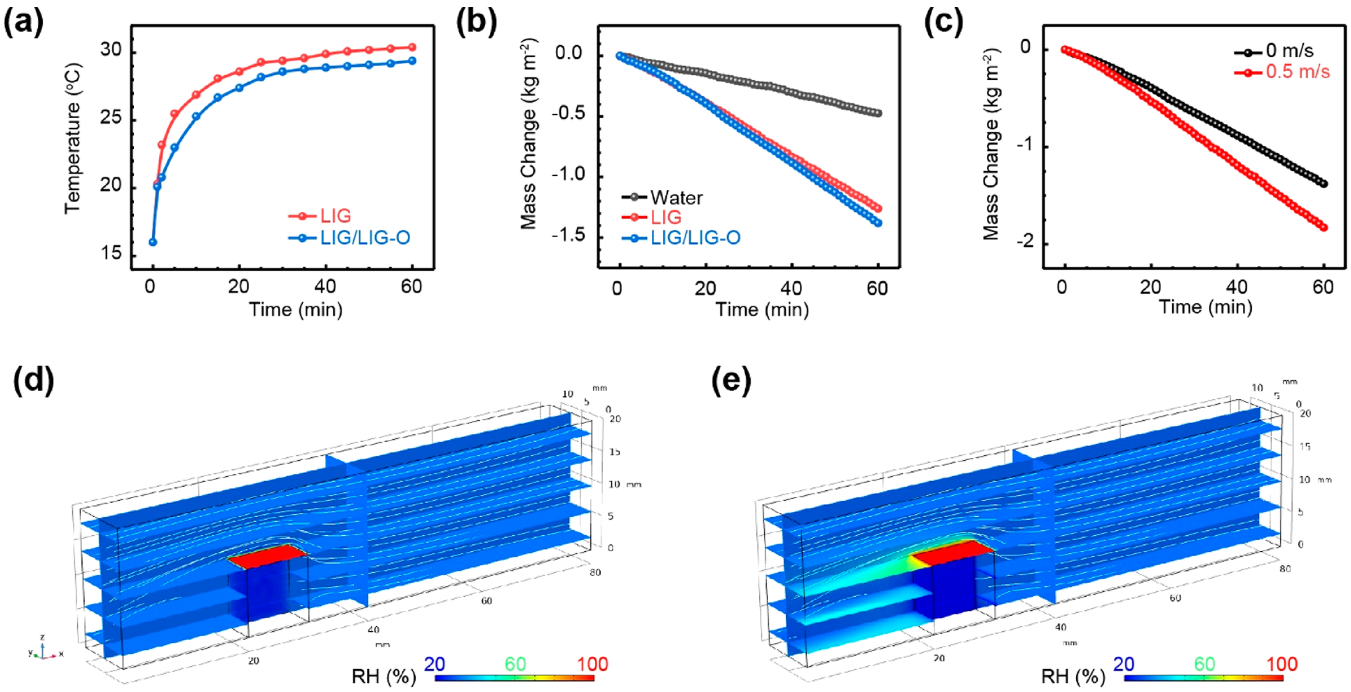

Figure 4. Solar interfacial evaporation performance under a solar irradiation of 1 kW m^{-2}. (a) Temperature vs time of the LIG membrane surface and Janus LIG/LIG-O membrane of upper LIG side. (b) Time-dependent mass change of water using LIG membrane and Janus LIG/LIG-O membrane. (c) Time-dependent mass change of water using Janus LIG/LIG-O membrane under airflow (v = 0 and 0.5 m/s). COMSOL simulation of relative humidity (RH) distribution around the evaporation surface (d) without airflow and (e) under airflow (v = 0.5 m/s).

by the laser processing parameters. The LIG exhibited a small reflectance (~9.5%) and negligible transmittance (~0%) in the range from 300 to 2000 nm (Figures S6 and S7), indicating a solar absorption of 90.5% (Figure 2g).

3.3. Antirotating and Windproof Abilities. To investigate the adhesive interaction between the LIG and LIG-O with water, we performed static and dynamic wetting characterizations. First, the Janus LIG/LIG-O membrane was cut into 5 mm × 10 mm and fixed on a stick. Next, the Janus LIG/LIG-O membrane was plunged into an air−water interface (Figure 3a). Interestingly, the upper hydrophobic LIG surface could prevent water wetting, which resulted in buoyancy and air trapping. In contrast with the hydrophobic LIG surface, the hydrophilic LIG-O surface demonstrated remarkable water adhesion. Meanwhile, the liquid bridge was formatted between the LIG-O surface and water when the LIG-O surface was withdrawn from the water surface (Figure 3b).

The floating Janus membrane was systematically tested to reveal its antirotating and windproof abilities. As shown in Figure 3c, a pentastar-shaped LIG/LIG-O membrane was distributed on the air−water interface. The LIG/LIG-O membrane remained in its initial state and did not flip over after the water surface rocked. As illustrated in Figure 3d, artificial wind was employed on the water surface. The LIG/LIG-O membranes adhered tightly to the water surface. Furthermore, owing to the Janus wettability of the LIG/LIG-O membrane, the membrane was preserved successfully after the wind blowing (Figure 3e).

3.4. Solar Interfacial Evaporation Performance. Hence, the Janus LIG/LIG-O membrane proved to be useful in solar interfacial evaporation enhancement. To characterize solar interfacial evaporation performances, the temperature change of the LIG and LIG/LIG-O membrane under simulated solar light (1 kW m^{-2}) was measured. Initially, the LIG and LIG/LIG-O membrane exhibited the ambient temperature (~16 °C). Based on our measurements, the surface temperature of the LIG could reash 30.4 °C, whereas the surface temperature of the LIG-O (29.4 °C) is lower than that of the LIG because water evaporation cooled the surface of the LIG/LIG-O (Figure 4a). In addition, mass changes were measured to study the evaporation rate. The evaporation rate of water, LIG (v = 0 m/s), LIG/LIG-O (v = 0 m/s), and LIG/LIG-O (v = 0.5 m/s) in the dark is 0.089, 0.165, 0.188, and 0.317 kg m^{-2} h^{-1}, respectively. As shown in Figure 4b, results indicated that the water evaporation rate of the LIG and LIG/LIG-O membrane could reach 1.095 and 1.191 kg m^{-2} h^{-1}. The solar thermal conversion efficiency (η) of LIG and LIG/LIG-O membrane is 70.46% and 76.5%, which is one of the best results among double layered graphene evaporators.[19,36,41,53,54] This superior performance in solar interfacial evaporation primarily is mainly attributed to the high solar absorption and Janus wettability. Importantly, as shown in the Figure 4c, the water evaporation rate of the LIG/LIG-O membrane could be improved to 1.512 kg m^{-2} h^{-1} under air blowing (v = 0.5 m/s). Airflow took evaporated water molecules away and reduced the relative humidity around the evaporation surface leading to the water evaporation rate improvement (Figure 4d,e). In addition, the parasitic evaporation from container sides is analyzed. The radius of cylinder container used in solar evaporation tests is 1 cm. The area of the water evaporation is about ~3.14 cm^2. The net water evaporation rate is 0.384 kg m^{-2} h^{-1}. As for the LIG/LIG-O membrane (v = 0.5 m/s), the area of the membrane is 1 cm^2. Therefore, the parasitic evaporation from container sides is ~0.103 g h^{-1}. The net water evaporation rate of LIG/LIG-O membranes (v = 0.5 m/s, 1.512 kg m^{-2} h^{-1} cm^{-2}) has considered the parasitic evaporation from container sides. In

https://dx.doi.org/10.1021/acsami.0c05401
ACS Appl. Mater. Interfaces 2020, 12, 25435−25443

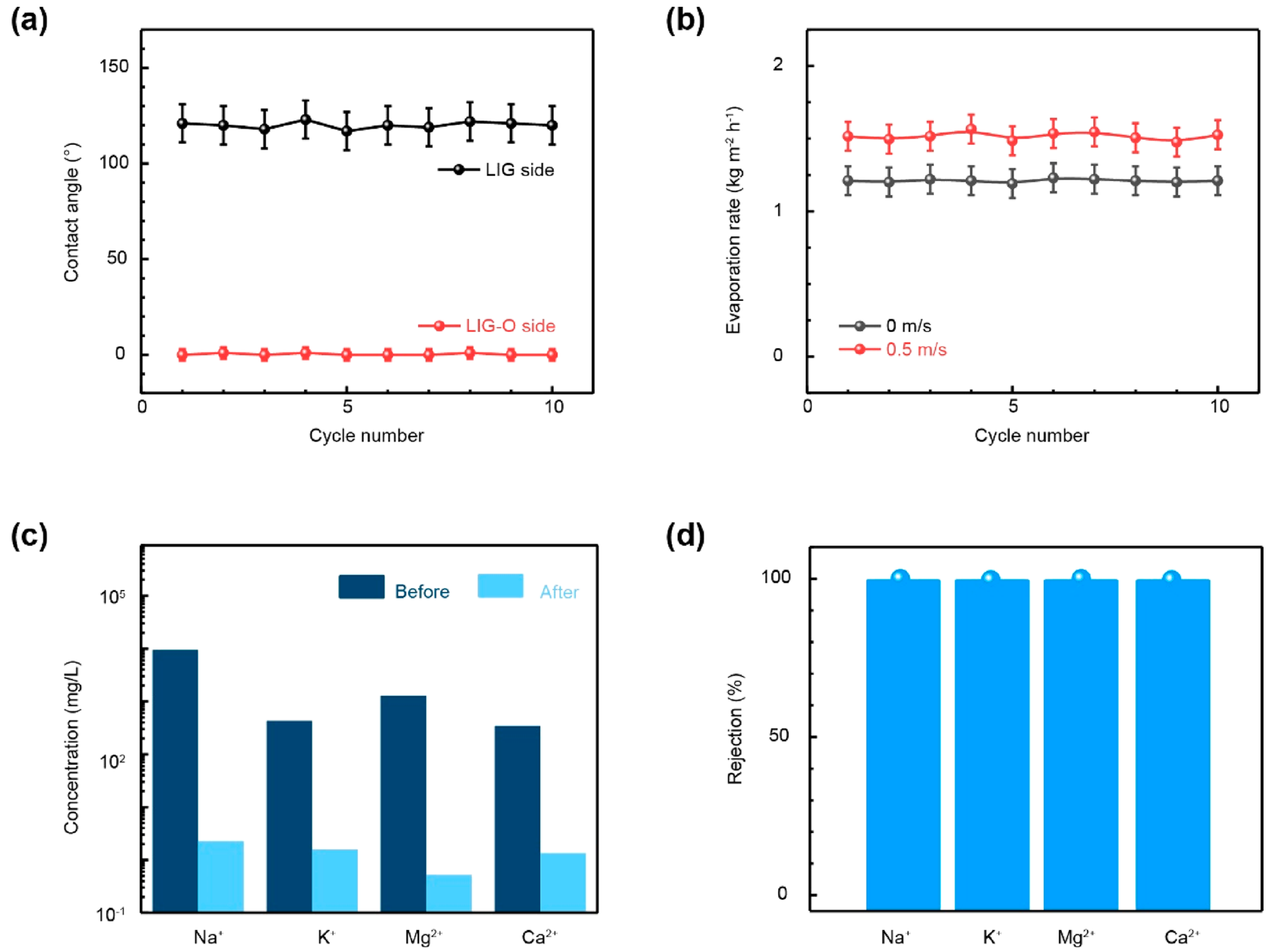

Figure 5. Ion rejection performance. (a) Janus wettability of the Janus LIG/LIG-O membrane over 10 cycles. (b) Evaporation rate of Janus LIG/LIG-O membrane for 60 min over 10 cycles under airflow (v = 0 and 0.5 m/s), demonstrating the reusability of the LIG/LIG-O membrane. (c and d) the measured concentration and the ion rejection before and after desalination.

this study, we focused on the air flow approach to achieve highly efficient solar evaporation, and the Janus LIG/LIG-O membrane is a proof of concept for solar evaporation. Therefore, among the graphene-based multilayered structures for solar interfacial evaporation, we achieved a higher evaporation rate in this study because the previous reports did not include air flow. This may be attributed to the air flowing enhancement approach and the combination of microscale capillary water transporting and nanoscale light trapping.

Additionally, Figure 5a,b shows that the water evaporation rate and wettability of LIG/LIG-O membrane underwent 10 cycles without noticeable decrease, which might be caused by the single-material-based membrane. The target application of our Janus photothermal membrane is seawater desalination. To evalue the desalination ability of the LIG/LIG-O membrane, seawater containing Na^+, K^+, Mg^{2+}, and Ca^{2+} was used. Figure S8 is the schematic illustration of the device for water liquid production. As shown in Figure 5c,d, the concentration of these ions would decrease by 3−4 orders of magnitude with ion rejection nearly 100% after the desalination.

4. CONCLUSIONS

In conclusion, we developed a hydrophobic/hydrophilic solar interfacial evaporation membrane by designing and fabricating a LIG/LIG-O based membrane. Benefiting from the Janus wettability, the LIG/LIG-O membrane demonstrates interfacial floatability improvement and hence antirotating and windproof abilities. More importantly, chemical-free procedures and a water evaporation rate of 1.512 kg m^{-2} h^{-1} were demonstrated by air flowing enhancement under 1 kW m^{-2}. In addition, our proposed method is simple and does not require complicated chemical processes. The membrane demonstrated excellent stability because the entire membrane was fabricated based on a single LIG membrane, and the evaporation efficiently removed heat to avoid thermal loss. The high-water evaporation rate of LIG rendered it a promising material for water purification and seawater desalination.

■ ASSOCIATED CONTENT

Supporting Information

The Supporting Information is available free of charge at https://pubs.acs.org/doi/10.1021/acsami.0c05401.

Laser patterning of LIG, i.e., the school badge of Jilin University; the yellow region is the PI and the black region is the LIG.; Raman spectrum of LIG; survey spectrum of the LIG side; survey spectrum of the LIG-O side; C 1s XPS of the LIG and LIG-O sides; reflectance spectrum of the LIG; transmittance spectrum of the

https://dx.doi.org/10.1021/acsami.0c05401
ACS Appl. Mater. Interfaces 2020, 12, 25435−25443

LIG; and schematic illustration of the device for water liquid production (PDF)

AUTHOR INFORMATION

Corresponding Author

Yong-Lai Zhang − *State Key Laboratory of Integrated Optoelectronics, College of Electronic Science and Engineering, Jilin University, Changchun 130012, China;* orcid.org/0000-0002-4282-250X; Email: yonglaizhang@jlu.edu.cn

Authors

Dong-Dong Han − *State Key Laboratory of Integrated Optoelectronics, College of Electronic Science and Engineering and Key Laboratory of Automobile Materials Ministry of Education, College of Materials Science & Engineering, and Electron Microscopy Center, Jilin University, Changchun 130012, China*

Zhao-Di Chen − *State Key Laboratory of Integrated Optoelectronics, College of Electronic Science and Engineering, Jilin University, Changchun 130012, China*

Ji-Chao Li − *State Key Laboratory of Integrated Optoelectronics, College of Electronic Science and Engineering, Jilin University, Changchun 130012, China*

Jiang-Wei Mao − *State Key Laboratory of Integrated Optoelectronics, College of Electronic Science and Engineering, Jilin University, Changchun 130012, China*

Zhi-Zhen Jiao − *State Key Laboratory of Integrated Optoelectronics, College of Electronic Science and Engineering, Jilin University, Changchun 130012, China*

Wei Wang − *State Key Laboratory of Integrated Optoelectronics, College of Electronic Science and Engineering, Jilin University, Changchun 130012, China*

Wei Zhang − *Key Laboratory of Automobile Materials Ministry of Education, College of Materials Science & Engineering, and Electron Microscopy Center, Jilin University, Changchun 130012, China;* orcid.org/0000-0002-6414-7015

Hong-Bo Sun − *State Key Laboratory of Precision Measurement Technology and Instruments, Department of Precision Instrument, Tsinghua University, Haidian, Beijing 00084, China*

Complete contact information is available at: https://pubs.acs.org/10.1021/acsami.0c05401

Author Contributions

The manuscript was written through contributions of all authors. All authors have given approval to the final version of the manuscript.

Notes

The authors declare no competing financial interest.

ACKNOWLEDGMENTS

This work was supported by the National Key Research and Development Program of China and National Natural Science Foundation of China (NSFC) under Grant Nos. 2017YFB1104600, 61905087, 61935008, 61775078, and 61590930. Scientific and Technological Developing Scheme of Jilin Province Nos. 20180101061JC.

REFERENCES

(1) Zhao, F.; Zhou, X. Y.; Shi, Y.; Qian, X.; Alexander, M.; Zhao, X. P.; Mendez, S.; Yang, R. G.; Qu, L. T.; Yu, G. H. Highly Efficient Solar Vapour Generation via Hierarchically Nanostructured Gels. *Nat. Nanotechnol.* **2018**, *13*, 489.

(2) Ghasemi, H.; Ni, G.; Marconnet, A. M.; Loomis, J.; Yerci, S.; Miljkovic, N.; Chen, G. Solar Steam Generation by Heat Localization. *Nat. Commun.* **2014**, *5*, 4449.

(3) You, R.; Liu, Y. Q.; Hao, Y. L.; Han, D. D.; Zhang, Y. L.; You, Z. Laser Fabrication of Graphene-Based Flexible Electronics. *Adv. Mater.* **2020**, *32*, 1901981.

(4) Zhang, Z. H.; Li, X. M.; Yin, J.; Xu, Y.; Fei, W. W.; Xue, M. M.; Wang, Q.; Zhou, J. X.; Guo, W. L. Emerging Hydrovoltaic Technology. *Nat. Nanotechnol.* **2018**, *13*, 1109−1119.

(5) Tao, P.; Ni, G.; Song, C. Y.; Shang, W.; Wu, J. B.; Zhu, J.; Chen, G.; Deng, T. Solar-Driven Interfacial Evaporation. *Nat. Energy* **2018**, *3*, 1031−1041.

(6) Han, M.; Kim, B.; Lim, H.; Jang, H.; Kim, E. Transparent Photothermal Heaters From a Soluble NIR-Absorbing Diimmonium Salt. *Adv. Mater.* **2020**, *32*, 1905096.

(7) Yang, Y.; Zhao, R. Q.; Zhang, T. F.; Zhao, K.; Xiao, P. S.; Ma, Y. F.; Ajayan, P. M.; Shi, G. Q.; Chen, Y. S. Graphene-Based Standalone Solar Energy Converter for Water Desalination and Purification. *ACS Nano* **2018**, *12*, 829−835.

(8) Zhou, X. Y.; Zhao, F.; Guo, Y. H.; Zhang, Y.; Yu, G. H. A Hydrogel-Based Antifouling Solar Evaporator for Highly Efficient Water Desalination. *Energy Environ. Sci.* **2018**, *11*, 1985−1992.

(9) Chen, C. J.; Kuang, Y. D.; Hu, L. B. Challenges and Opportunities for Solar Evaporation. *Joule* **2019**, *3*, 683−718.

(10) Wu, X.; Gao, T.; Han, C. H.; Xu, J. S.; Owens, G.; Xu, H. L. A Photothermal Reservoir for Highly Efficient Solar Steam Generation Without Bulk Water. *Sci. Bull.* **2019**, *64*, 1625−1633.

(11) Zhang, P. P.; Liu, F.; Liao, Q. H.; Yao, H. Z.; Geng, H. Y.; Cheng, H. H.; Li, C.; Qu, L. T. A Microstructured Graphene/Poly(N-Isopropylacrylamide) Membrane for Intelligent Solar Water Evaporation. *Angew. Chem., Int. Ed.* **2018**, *57*, 16343−16347.

(12) Bao, X.; Yuan, Y.; Chen, J. Q.; Zhang, B. H.; Li, D.; Zhou, D.; Jing, P. T.; Xu, G. Y.; Wang, Y. L.; Hola, K.; Shen, D. Z.; Wu, C. F.; Song, L.; Liu, C. B.; Zboril, R.; Qu, S. N. In Vivo Theranostics with Near-Infrared-Emitting Carbon Dots-Highly Efficient Photothermal Therapy Based on Passive Targeting After Intravenous Administration. *Light: Sci. Appl.* **2018**, *7*, 91.

(13) Zhang, D. L.; Lan, L.; Bai, Y. R.; Majeed, H.; Kandel, M. E.; Popescu, G.; Cheng, J. X. Bond-Selective Transient Phase Imaging via Sensing of the Infrared Photothermal Effect. *Light: Sci. Appl.* **2019**, *8*, 116.

(14) Zhang, Y. L.; Ma, J. N.; Liu, S.; Han, D. D.; Liu, Y. Q.; Chen, Z. D.; Mao, J. W.; Sun, H. B. A "Yin"-"Yang" Complementarity Strategy for Design and Fabrication of Dual-Responsive Bimorph Actuators. *Nano Energy* **2020**, *68*, 104302.

(15) Wang, W.; Liu, Y. Q.; Liu, Y.; Han, B.; Wang, H.; Han, D. D.; Wang, J. N.; Zhang, Y. L.; Sun, H. B. Direct Laser Writing of Superhydrophobic PDMS Elastomers for Controllable Manipulation via Marangoni Effect. *Adv. Funct. Mater.* **2017**, *27*, 1702946.

(16) Xin, W.; Li, X. K.; He, X. L.; Su, B. W.; Jiang, X. Q.; Huang, K. X.; Zhou, X. F.; Liu, Z. B.; Tian, J. G. Black-Phosphorus-Based Orientation-Induced Diodes. *Adv. Mater.* **2018**, *30*, 1704653.

(17) Guo, Y. H.; Zhao, F.; Zhou, X. Y.; Chen, Z. C.; Yu, G. H. Tailoring Nanoscale Surface Topography of Hydrogel for Efficient Solar Vapor Generation. *Nano Lett.* **2019**, *19*, 2530−2536.

(18) Li, W. G.; Li, Z.; Bertelsmann, K.; Fan, D. E. Portable Low-Pressure Solar Steaming-Collection Unisystem with Polypyrrole Origamis. *Adv. Mater.* **2019**, *31*, 1900720.

(19) Wang, Y.; Wang, C.; Song, X.; Megarajan, S. K.; Jiang, H. Improved Light-Harvesting and Thermal Management for Efficient Solar-Driven Water Evaporation Using 3D Photothermal Cones. *J. Mater. Chem. A* **2018**, *6*, 963.

(20) Shi, Y.; Li, R. Y.; Jin, Y.; Zhuo, S. F.; Shi, L.; Chang, J.; Hong, S.; Ng, K. C.; Wang, P. A 3D Photothermal Structure Toward Improved Energy Efficiency in Solar Steam Generation. *Joule* **2018**, *2*, 1171−1186.

https://dx.doi.org/10.1021/acsami.0c05401
ACS Appl. Mater. Interfaces 2020, 12, 25435−25443

(21) Malinauskas, M.; Zukauskas, A.; Hasegawa, S.; Hayasaki, Y.; Mizeikis, V.; Buividas, R.; Juodkazis, S. Ultrafast Laser Processing of Materials: From Science to Industry. *Light: Sci. Appl.* **2016**, *5*, No. e16133.

(22) Li, C. W.; Jiang, D. G.; Huo, B. B.; Ding, M. C.; Huang, C. C.; Jia, D. D.; Li, H. X.; Liu, C. Y.; Liu, J. Q. Scalable and Robust Bilayer Polymer Foams for Highly Efficient and Stable Solar Desalination. *Nano Energy* **2019**, *60*, 841−849.

(23) Gao, S.; Dong, X.; Huang, J.; Dong, J.; Maggio, F. D.; Wang, S.; Guo, F.; Zhu, T.; Chen, Z.; Lai, Y. Bioinspired Soot-Deposited Janus Fabrics for Sustainable Solar Steam Generation with Salt-Rejection. *Glob. Chall.* **2019**, *3*, 1800117.

(24) Yang, Y. W.; Zhao, H. Y.; Yin, Z. Y.; Zhao, J. Q.; Yin, X. T.; Li, N.; Yin, D. D.; Li, Y. N.; Lei, B.; Du, Y. P.; Que, W. X. A General Salt-Resistant Hydrophilic/Hydrophobic Nanoporous Double Layer Design for Efficient and Stable Solar Water Evaporation Distillation. *Mater. Horiz.* **2018**, *5*, 1143−1150.

(25) Ma, X.; Fang, W. Z.; Guo, Y.; Li, Z. Y.; Chen, D. K.; Ying, W.; Xu, Z.; Gao, C.; Peng, X. S. Hierarchical Porous SWCNT Stringed Carbon Polyhedrons and PSS Threaded MOF Bilayer Membrane for Efficient Solar Vapor Generation. *Small* **2019**, *15*, 1900354.

(26) Yang, Y. B.; Yang, X. D.; Fu, L. N.; Zou, M. C.; Cao, A. Y.; Du, Y. P.; Yuan, Q.; Yan, C. H. Two-Dimensional Flexible Bilayer Janus Membrane for Advanced Photothermal Water Desalination. *ACS Energy Lett.* **2018**, *3*, 1165−1171.

(27) Gao, T. T.; Li, Y. J.; Chen, C. J.; Yang, Z.; Kuang, Y. D.; Jia, C.; Song, J. W.; Hitz, E. M.; Liu, B. Y.; Huang, H.; Yu, J. Y.; Yang, B.; Hu, L. B. Architecting a Floatable, Durable, and Scalable Steam Generator: Hydrophobic/Hydrophilic Bifunctional Structure for Solar Evaporation Enhancement. *Small Methods* **2019**, *3*, 1800176.

(28) Xu, W. C.; Hu, X. Z.; Zhuang, S. D.; Wang, Y. X.; Li, X. Q.; Zhou, L.; Zhu, S. N.; Zhu, J. Flexible and Salt Resistant Janus Absorbers by Electrospinning for Stable and Efficient Solar Desalination. *Adv. Energy Mater.* **2018**, *8*, 1702884.

(29) Zhang, Q.; Yi, G.; Fu, Z.; Yu, H. T.; Chen, S.; Quan, X. Vertically Aligned Janus MXene-Based Aerogels for Solar Desalination with High Efficiency and Salt Resistance. *ACS Nano* **2019**, *13*, 13196−13207.

(30) Hu, R.; Zhang, J. Q.; Kuang, Y. D.; Wang, K. B.; Cai, X. Y.; Fang, Z. Q.; Huang, W. Q.; Chen, G.; Wang, Z. X. A Janus Evaporator with Low Tortuosity for Long-Term Solar Desalination. *J. Mater. Chem. A* **2019**, *7*, 15333−15340.

(31) Jiang, S. J.; Hu, Y. L.; Wu, H.; Zhang, Y. C.; Zhang, Y. Y.; Wang, Y. L.; Zhang, Y. H.; Zhu, W. L.; Li, J. W.; Wu, D.; Chu, J. R. Multifunctional Janus Microplates Arrays Actuated by Magnetic Fields for Water/Light Switches and Bio-Inspired Assimilatory Coloration. *Adv. Mater.* **2019**, *31*, 1807507.

(32) Yang, H. C.; Xie, Y. S.; Hou, J. W.; Cheetham, A. K.; Chen, V.; Darling, S. B. Janus Membranes: Creating Asymmetry for Energy Efficiency. *Adv. Mater.* **2018**, *30*, 1801495.

(33) Yang, H. C.; Chen, Z. W.; Xie, Y. S.; Wang, J.; Elam, J. W.; Li, W. H.; Darling, S. B. Chinese Ink: A Powerful Photothermal Material for Solar Steam Generation. *Adv. Mater. Interfaces* **2019**, *6*, 1801252.

(34) Xia, Z. J.; Yang, H. C.; Chen, Z. W.; Waldman, R. Z.; Zhao, Y. S.; Zhang, C.; Patel, S. N.; Darling, S. B. Porphyrin Covalent Organic Framework (POF)-Based Interface Engineering for Solar Steam Generation. *Adv. Mater. Interfaces* **2019**, *6*, 1900254.

(35) Zhang, H.; Li, L.; Jiang, B.; Zhang, Q.; Ma, J.; Tang, D.; Song, Y. Highly Thermally Insulated and Superhydrophilic Corn Straw for Efficient Solar Vapor Generation. *ACS Appl. Mater. Interfaces* **2020**, *12*, 16503−16511.

(36) Zhang, Q.; Yang, H. J.; Xiao, X. F.; Wang, H.; Yan, L.; Shi, Z. X.; Chen, Y. L.; Xu, W. L.; Wang, X. B. A New Self-Desalting Solar Evaporation System Based on a Vertically Oriented Porous Polyacrylonitrile Foam. *J. Mater. Chem. A* **2019**, *7*, 14620−14628.

(37) Wang, F.; Wei, D. Y.; Li, Y. Z.; Chen, T.; Mu, P.; Sun, H. X.; Zhu, Z. Q.; Liang, W. D.; Li, A. Chitosan/Reduced Graphene Oxide-Modified Spacer Fabric as A Salt-Resistant Solar Absorber for Efficient Solar Steam Generation. *J. Mater. Chem. A* **2019**, *7*, 18311−18317.

(38) Huo, B. B.; Jiang, D. G.; Cao, X. Y.; Liang, H.; Liu, Z.; Li, C. W.; Liu, J. Q. N-Doped Graphene/Carbon Hybrid Aerogels for Efficient Solar Steam Generation. *Carbon* **2019**, *142*, 13−19.

(39) Cao, Z. X.; Yao, B. C.; Qin, C. Y.; Yang, R.; Guo, Y. H.; Zhang, Y. F.; Wu, Y.; Bi, L.; Chen, Y. F.; Xie, Z. D.; Peng, G. D.; Huang, S. W.; Wong, C. W.; Rao, Y. J. Biochemical Sensing in Graphene-Enhanced Microfiber Resonators with Individual Molecule Sensitivity and Selectivity. *Light: Sci. Appl.* **2019**, *8*, 107.

(40) Zhang, Y. L.; Liu, Y. Q.; Han, D. D.; Ma, J. N.; Wang, D.; Li, X. B.; Sun, H. B. Quantum-Confined-Superfluidics-Enabled Moisture Actuation Based on Unilaterally Structured Graphene Oxide Papers. *Adv. Mater.* **2019**, *31*, 1901585.

(41) Wang, G.; Fu, Y.; Ma, X. F.; Pi, W. B.; Liu, D. W.; Wang, X. B. Reusable Reduced Graphene Oxide Based Double-Layer System Modified by Polyethylenimine for Solar Steam Generation. *Carbon* **2017**, *114*, 117−124.

(42) Hong, S. H.; Shi, Y.; Li, R. Y.; Zhang, C. L.; Jin, Y.; Wang, P. Nature-Inspired, 3D Origami Solar Steam Generator Toward Near Full Utilization of Solar Energy. *ACS Appl. Mater. Interfaces* **2018**, *10*, 28517−28524.

(43) Li, G. J.; Law, W. C.; Chan, K. C. Floating, Highly Efficient, and Scalable Graphene Membranes for Seawater Desalination Using Solar Energy. *Green Chem.* **2018**, *20*, 3689−3695.

(44) Zhang, Q.; Xiao, X. F.; Wang, G.; Ming, X.; Liu, X. H.; Wang, H.; Yang, H. J.; Xu, W. L.; Wang, X. B. Silk-Based Systems for Highly Efficient Photothermal Conversion Under One Sun: Portability, Flexibility, and Durability. *J. Mater. Chem. A* **2018**, *6*, 17212−17219.

(45) Hao, W.; Chiou, K.; Qiao, Y. M.; Liu, Y. M.; Song, C. Y.; Deng, T.; Huang, J. X. Crumpled Graphene Ball-Based Broadband Solar Absorbers. *Nanoscale* **2018**, *10*, 6306−6312.

(46) Cui, L. F.; Zhang, P. P.; Xiao, Y. K.; Liang, Y.; Liang, H. X.; Cheng, Z. H.; Qu, L. T. High Rate Production of Clean Water Based on the Combined Photo-Electro-Thermal Effect of Graphene Architecture. *Adv. Mater.* **2018**, *30*, 1706805.

(47) Zhang, P. P.; Li, J.; Lv, L. X.; Zhao, Y.; Qu, L. T. Vertically Aligned Graphene Sheets Membrane for Highly Efficient Solar Thermal Generation of Clean Water. *ACS Nano* **2017**, *11*, 5087−5093.

(48) Liang, H. X.; Liao, Q. H.; Chen, N.; Liang, Y.; Lv, G. Q.; Zhang, P. P.; Lu, B.; Qu, L. T. Thermal Efficiency of Solar Steam Generation Approaching 100% Through Capillary Water Transport. *Angew. Chem., Int. Ed.* **2019**, *58*, 19041.

(49) Li, X. Q.; Lin, R. X.; Ni, G.; Xu, N.; Hu, X. Z.; Zhu, B.; Lv, G. X.; Li, J. L.; Zhu, S. N.; Zhu, J. Three-Dimensional Artificial Transpiration for Efficient Solar Waste-Water Treatment. *Natl. Sci. Rev.* **2018**, *5*, 70−77.

(50) Li, X. Q.; Xu, W. C.; Tang, M. Y.; Zhou, L.; Zhu, B.; Zhu, S. N.; Zhu, J. Graphene Oxide-Based Efficient and Scalable Solar Desalination Under One Sun with a Confined 2D Water Path. *Proc. Natl. Acad. Sci. U. S. A.* **2016**, *113*, 13953−13958.

(51) Hu, X. Z.; Xu, W. C.; Zhou, L.; Tan, Y. L.; Wang, Y.; Zhu, S. N.; Zhu, J. Tailoring Graphene Oxide-Based Aerogels for Efficient Solar Steam Generation Under One Sun. *Adv. Mater.* **2017**, *29*, 1604031.

(52) Li, Y. J.; Gao, T. T.; Yang, Z.; Chen, C. J.; Kuang, Y. D.; Song, J. W.; Jia, C.; Hitz, E. M.; Yang, B.; Hu, L. B. Graphene Oxide-Based Evaporator with One-Dimensional Water Transport Enabling High-Efficiency Solar Desalination. *Nano Energy* **2017**, *41*, 201−209.

(53) Li, Y. J.; Gao, T. T.; Yang, Z.; Chen, C. J.; Luo, W.; Song, J. W.; Hitz, E.; Jia, C.; Zhou, Y. B.; Liu, B. Y.; Yang, B.; Hu, L. B. 3D-Printed, All-In-One Evaporator for High-Efficiency Solar Steam Generation Under 1 Sun Illumination. *Adv. Mater.* **2017**, *29*, 1700981.

(54) Guo, A. K.; Ming, X.; Fu, Y.; Wang, G.; Wang, X. B. Fiber-Based, Double-Sided, Reduced Graphene Oxide Films for Efficient Solar Vapor Generation. *ACS Appl. Mater. Interfaces* **2017**, *9*, 29958−29964.

(55) Zhang, P. P.; Liao, Q. H.; Yao, H. Z.; Cheng, H. H.; Huang, Y. X.; Yang, C.; Jiang, L.; Qu, L. T. Three-Dimensional Water Evaporation on a Macroporous Vertically Aligned Graphene Pillar Array Under One Sun. *J. Mater. Chem. A* **2018**, *6*, 15303−15309.

(56) Bai, B. L.; Yang, X. H.; Tian, R.; Ren, W. C.; Suo, R.; Wang, H. B. High-Efficiency Solar Steam Generation Based on Blue Brick-Graphene Inverted Cone Evaporator. *Appl. Therm. Eng.* **2019**, *163*, 114379.

(57) Sun, H. X.; Li, Y. Z.; Zhu, Z. Q.; Mu, P.; Wang, F.; Liang, W. D.; Ma, C. H.; Li, A. Photothermal Conversion Material Derived from Used Cigarette Filters for Solar Steam Generation. *ChemSusChem* **2019**, *12*, 4257−4264.

(58) Zhu, L. L.; Gao, M. M.; Peh, C. K. N.; Ho, G. W. Recent Progress in Solar-Driven Interfacial Water Evaporation: Advanced Designs and Applications. *Nano Energy* **2019**, *57*, 507−518.

(59) Ren, H. Y.; Tang, M.; Guan, B. L.; Wang, K. X.; Yang, J. W.; Wang, F. F.; Wang, M. Z.; Shan, J. Y.; Chen, Z. L.; Wei, D.; Peng, H. L.; Liu, Z. F. Hierarchical Graphene Foam for Efficient Omnidirectional Solar-Thermal Energy Conversion. *Adv. Mater.* **2017**, *29*, 1702590.

(60) Zhao, Y. Y.; Yu, C. M.; Lan, H.; Cao, M. Y.; Jiang, L. Improved Interfacial Floatability of Superhydrophobic/Superhydrophilic Janus Sheet Inspired by Lotus Leaf. *Adv. Funct. Mater.* **2017**, *27*, 1701466.

(61) Lin, J.; Peng, Z. W.; Liu, Y. Y.; Ruiz-Zepeda, F.; Ye, R. Q.; Samuel, E. L. G.; Yacaman, M. J.; Yakobson, B. I.; Tour, J. M. Laser-Induced Porous Graphene Films From Commercial Polymers. *Nat. Commun.* **2014**, *5*, 5714.

(62) Zhang, B. Y.; Song, C. Y.; Liu, C.; Min, J. K.; Azadmanjiri, J.; Ni, Y. X.; Niu, R.; Gong, J.; Zhao, Q.; Tang, T. Molten Salts Promoting the "Controlled Carbonization" of Waste Polyesters Into Hierarchically Porous Carbon for High-Performance Solar Steam Evaporation. *J. Mater. Chem. A* **2019**, *7*, 22912−22923.

(63) Gong, J.; Chen, X. C.; Tang, T. Recent Progress in Controlled Carbonization of (Waste) Polymers. *Prog. Polym. Sci.* **2019**, *94*, 1−32.

(64) Zhang, J. B.; Ren, M. Q.; Wang, L. Q.; Li, Y. L.; Yakobson, B. I.; Tour, J. M. Oxidized Laser-Induced Graphene for Efficient Oxygen Electrocatalysis. *Adv. Mater.* **2018**, *30*, 1707319.

(65) Balandin, A. A.; Ghosh, S.; Bao, W. Z.; Calizo, I.; Teweldebrhan, D.; Miao, F.; Lau, C. N. Superior Thermal Conductivity of Single-Layer Graphene. *Nano Lett.* **2008**, *8*, 902−907.

(66) Balandin, A. A. Thermal Properties of Graphene and Nanostructured Carbon Materials. *Nat. Mater.* **2011**, *10*, 569−581.

(67) Renteria, J. D.; Ramirez, S.; Malekpour, H.; Alonso, B.; Centeno, A.; Zurutuza, A.; Cocemasov, A. I.; Nika, D. L.; Balandin, A. A. Strongly Anisotropic Thermal Conductivity of Free-Standing Reduced Graphene Oxide Films Annealed at High Temperature. *Adv. Funct. Mater.* **2015**, *25*, 4664−4672.

(68) Yang, J. L.; Pang, Y. S.; Huang, W. X.; Shaw, S. K.; Schiffbauer, J.; Pillers, M. A.; Mu, X.; Luo, S. R.; Zhang, T.; Huang, Y. J.; Li, G. X.; Ptasinska, S.; Lieberman, M.; Luo, T. F. Functionalized Graphene Enables Highly Efficient Solar Thermal Steam Generation. *ACS Nano* **2017**, *11*, 5510−5518.

(69) Ito, Y.; Tanabe, Y.; Han, J. H.; Fujita, T.; Tanigaki, K.; Chen, M. W. Multifunctional Porous Graphene for High-Efficiency Steam Generation by Heat Localization. *Adv. Mater.* **2015**, *27*, 4302−4307.

(70) Xu, N.; Li, J. L.; Wang, Y.; Fang, C.; Li, X. Q.; Wang, Y. X.; Zhou, L.; Zhu, B.; Wu, Z.; Zhu, S. N.; Zhu, J. A Water Lily-Inspired Hierarchical Design for Stableand Efficient Solar Evaporation of High-Salinity Brine. *Sci. Adv.* **2019**, *5*, No. eaaw7013.

(71) Song, X. Y.; Song, H. C.; Wang, S.; Liu, J. J.; Zhou, L.; Xu, J.; Chen, K. J. Enhancement of Solar Vapor Generation by a 3D Hierarchical Heat Trapping Structure. *J. Mater. Chem. A* **2019**, *7*, 26496−26503.

(72) Zhao, F.; Guo, Y. H.; Zhou, X. Y.; Shi, W.; Yu, G. H. Materials for Solar-Powered Water Evaporation. *Nat. Rev. Mater.* **2020**, *5*, 388.

(73) Cao, S.; Jiang, Q.; Wu, X.; Ghim, D.; Gholami Derami, H.; Chou, P.-I.; Jun, Y.-S.; Singamaneni, S. Advances in Solar Evaporator Materials for Freshwater Generation. *J. Mater. Chem. A* **2019**, *7*, 24092−24123.